Available online at www.sciencedirect.com
ScienceDirect
Engineering Fracture Mechanics 74 (2007) 1928–1941
Engineering Fracture Mechanics
www.elsevier.com/locate/engfracmech

High-speed photography of compressed human trabecular bone correlates whitening to microscopic damage

P.J. Thurner [a,*], B. Erickson [a], R. Jungmann [a], Z. Schriock [a], J.C. Weaver [b], G.E. Fantner [a], G. Schitter [a], D.E. Morse [b], P.K. Hansma [a]

[a] Physics Department, Hansma Lab – Broida Hall, University of California, Santa Barbara, CA 93106, USA
[b] Department of Molecular, Cellular and Developmental Biology, University of California, Santa Barbara, CA, USA

Received 19 January 2006; received in revised form 21 May 2006; accepted 31 May 2006
Available online 4 August 2006

Abstract

Mechanical testing of trabecular bone is mainly motivated by the huge impact of osteoporosis in post-menopausal women and the aged in society in terms of social and health care costs. Trabecular bone loss and impairment of its mechanical properties reduce bone strength and increase fracture risk, especially in vertebrae. It is generally accepted that in addition to bone mineral density, microarchitecture and material properties of bone also play important roles for bone strength and fracture risk. In order to overcome the limitations of standard mechanical tests delivering merely integral information about complicated samples, experiments were designed for step-wise mechanical testing with concurrent imaging of trabecular and cortical bone. In this communication we present an approach for real-time imaging of trabecular bone during compression using high-speed photography and investigate the hypothesis whether the whitening of deformed trabeculae is due to microdamage. Experiments on human trabecular bone samples from a healthy male donor revealed that failure of such samples is highly localized in fracture bands. Moreover, strongly deformed trabeculae were seen to whiten, an effect similar to stress whitening in polymers. Scanning Electron Microscopy of the same regions of interest revealed that whitened trabeculae were strongly damaged by microscopic cracks and mostly failed in delamination. Higher resolution images uncovered mineralized collagen fibrils spanning the cracks. The whitening partially faded after unloading of the samples, presumably due to partial crack closure. Overall, high-speed photography enables microdamage detection in real-time during a mechanical test and provides a correlation to recorded stress strain curves.

Keywords: Trabecular bone; Fracture; High-speed photography; Stress-whitening; Microdamage; Delamination

1. Introduction

Mechanical testing of trabecular bone is a vast experimental field [3,6,11–14,31]. This research is mainly motivated by the reduction of bone strength due to osteoporosis, a systemic skeletal disease [10,18], which

* Corresponding author. Tel.: +1 805 893 3999. fax: +1 805 893 8315.
E-mail address: thurner@physics.ucsb.edu (P.J. Thurner).

0013-7944/$ - see front matter © 2006 Elsevier Ltd. All rights reserved.
doi:10.1016/j.engfracmech.2006.05.024

comes with a concomitant increase of fracture risk. Post-menopausal women and the elderly are affected by this disease, along with certain younger populations. Osteoporosis also has a huge impact on society as it results in immense health care costs (13.8 billions of US$ in the USA alone in 1995) [25].

Trabecular bone is situated at the end of the long bones and in the spinal column, where it fills all of the inner vertebral space. In the long bones it transfers loads from joint surfaces onto the midshaft of the bone; in lumbar vertebrae, trabecular bone carries and transfers about 90% of the applied load [16,27]. Thus a loss of trabecular bone and/or impairment of its mechanical properties reduce bone strength and increase fracture risk, especially in vertebrae. The definition of osteoporosis is still based on bone density, i.e. a density 2.5 standard deviations lower than the healthy young normal is considered osteoporotic [34]. While, this definition proves to be adequate for a large population [11,17,26,35] it fails to be accurate for the individual. In fact sometimes up to 90% of the variation in bone strength are left unexplained on an individual basis [4], indicating the severe limitations in assessing fracture risk in patients by measuring bone density. It is generally accepted that microarchitecture and material properties of bone also play an important role for bone strength and fracture risk.

Standard mechanical tests, however, deliver only integral information on a bone specimen and no information of local processes experienced in the elastic, yield, and post-yield region. Failure of trabecular bone can in this way only be assessed in a post-hoc fashion, investigating sections or fracture patterns. In order to close this gap, experiments have been devised combining mechanical testing and imaging (so called functional imaging) of trabecular and also cortical bone [2,19,22,23,29,30]. Such functional imaging approaches give direct insight into the translation of apparent strains in trabecular and cortical bone. In both cases apparent strain can result in a broad range of local strains. Most of these functional imaging approaches deliver 3D information, however, they all are time consuming and thus limited to slow, quasi-static testing and/or recording of only a few different states of a sample subjected to mechanical testing. In contrast, high-speed photography is designed to record very fast processes, which allows for uncovering the failure dynamics of bone samples subjected to mechanical testing in a 2D fashion in real time.

In this communication we present images as well as quantitative data of the whitening effect found in bone as a consequence of overloading. This whitening effect was, to the best of our knowledge, mentioned in literature only once by Currey [5], who hypothesized it to be due to microcracking but also stated that experimental evidence (not shown in [5]) was not conclusive. In order to investigate the hypothesis whether whitening of bone is due to microdamage, we built a custom mechanical testing system that was combined with a high-speed camera in order to image trabecular bone while being mechanically tested in compression. Our results show that whitening in trabecular bone occurs in strongly deformed regions and SEM images of these regions provide proof for our hypothesis that whitening is due to microdamage.

2. Materials and methods

2.1. Sample preparation

We investigated a total of 14 bone samples isolated from a previously healthy male donor 21 years of age with no diagnosed bone disease. Bone samples with a height of about 4 mm and a cross-sectional area of about 4.9 mm by 4.9 mm were cut from vertebrae using a bandsaw (Marmed Inc. Cleveland, OH, USA) under constant irrigation with tap water. The smaller sample dimension is oriented in the original principal load bearing direction. Bone marrow was extracted from the specimens using a jet of pressurized water. All bone samples were weighed and their exact dimensions after preparation were measured using a pair of calipers. Mean sample dimensions, mass and density are given in Table 1.

2.2. Mechanical testing

A photograph of the experimental setup including the high-speed camera system is shown in Fig. 1A. Compression testing of all samples was done using a custom-made mechanical testing device, consisting of a load frame and a piston driven by a stepper motor. The piston impinges onto the transparent sample chamber (shown in Fig. 1B), made from PMMA consisting of a frame and a plunger, which applies the displacement

Table 1
Mean ($N = 14$) specimen dimension, mass, apparent density, elastic modulus, yield stress and strain as well as failure stress and strain

Parameter	Average	Standard deviation
Width [mm]	4.84	0.09
Length [mm]	4.89	0.04
Height [mm]	4.18	0.22
Mass [mg]	38.3	5.8
Apparent density [g/cm^3]	0.39	0.06
Elastic modulus [MPa]	104	30
Yield stress [MPa]	5.4	1.4
Yield strain [%]	5.6	1.0
Failure stress [MPa]	6.1	1.6
Failure strain [%]	8.9	2.2

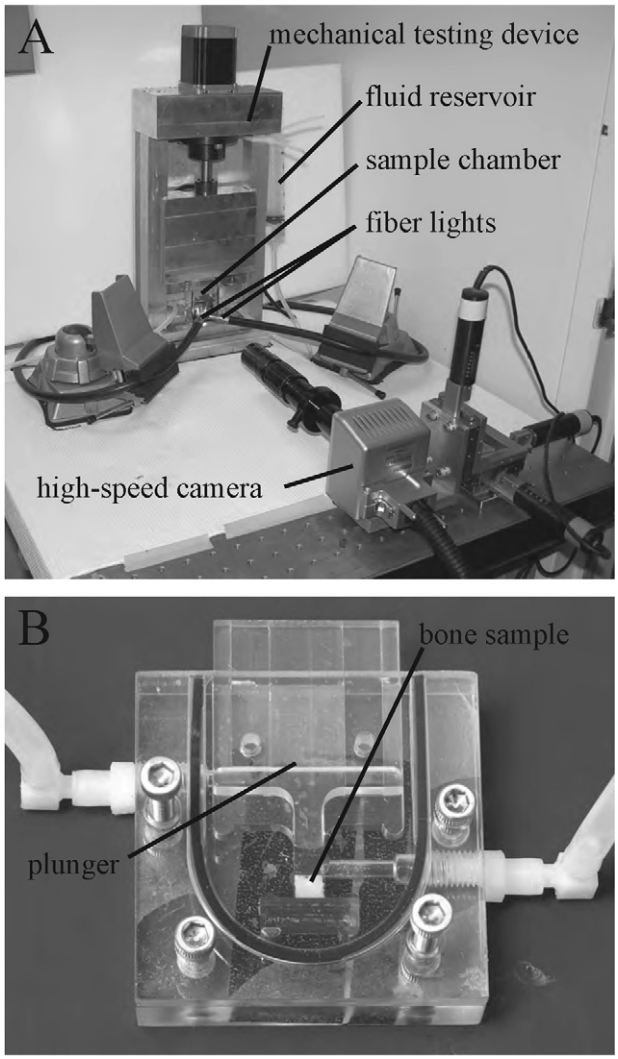

Fig. 1. Photograph of the custom mechanical testing device (A) used for the experiments. A high-speed camera is used to record the bone sample during compression. The sample is kept submerged in physiological buffer in a transparent sample holder (B).

onto the sample. The sample chamber has a fluid inlet and outlet, allowing for immersion of the specimen in fluid, in this case a buffer, containing 150 mM NaCl, and10 mM Hepes, at pH 7.0. The load exerted onto the sample was measured with a 100 lb capacity load cell (Model LBC-100, Transducer Techniques Inc., Temecula, CA, USA), which was mounted onto the lower end of the piston. Total displacement was measured with a laser distance sensor with 5 μm resolution (Baumer Electric OADM 12I6430/S35A, Frauenfeld, Switzerland). The experiment was controlled using a PC with an internal DAQ card (NI PCI-6013, National Instruments, Austin, TX, USA), an external I/O card (NI BNC 2110, National Instruments, Austin, TX, USA), and LabView (National Instruments, Austin, TX, USA). A strain rate of 50%/s was used for all mechanical tests. The mechanical tests consisted of two phases: in a first phase the piston was lowered slowly until a preload of 0.5 N was reached, in order to find the sample top. In a second phase the sample was then loaded at a constant strain rate up to 50% deformation. All stress strain curves were corrected for the toe regions they exhibited at low strains: a linear fit performed in the elastic region (i.e. the most linear region) of the stress strain curve was extrapolated and its intersection with zero stress was defined as the true zero strain. From these corrected stress strain curves, elastic modulus, yield stress and strain, as well as failure stress and strain were retrieved. Failure was defined as the first local maximum in each stress–strain curve. The average values of the extracted parameters are given in Table 1. In addition all stress–strain curves were re-sampled onto a common grid in order to compute an average stress strain curve for all 14 samples.

2.3. High-speed photography

We used an Ultima 512 high-speed camera (Photron Inc., San Diego, CA, USA) equipped with a KC lens, with a KC-AUX and an IF-3 lens mounted on top (Infinity, Boulder, CO, USA). The high-speed camera can record up to 32,000 frames/s but offers limited memory of 512 MB. We recorded images at 500 frames/s and a shutter opening time of 1/10,000 s as well as 60 frames/s and a shutter opening time of 1/12,000. The scene was illuminated from the front using two fiber lights (MH-100, Dolan Jenner Industries Inc., Lawrence, MA, USA) at angles of about $\pm 45°$ (cp. Fig. 1).

2.4. Image processing

All recorded movies where cropped to the region of the mechanical test using Image J (National Institute of Health, Bethesda, MD, USA). A texture correlation [1] algorithm was then applied using IDL (Research Systems Inc., Boulder, CO, USA) on the individual frames in order to detect the motion of the plunger. A region of interest with high contrast was selected on the plunger and tracked in subsequent recorded frames. The tracking allowed synchronization between recorded image data and stress–strain curves. For the quantification of whitening seen during compression of the samples, a thresholding algorithm, programmed in LabView was used. Due to flickering of the fiber lights during the experiments the threshold was determined from the histograms of five consecutive frames prior to compression, since five frames accounted for the approximate period of the intensity flickering. From each of the five histograms the highest pixel value (lying between 0 and 255) was determined. The average value of these five values was calculated and subsequently used as the threshold, i.e. all pixels having a higher value were counted as whitened pixels in each frame. Due to flickering of the fiber lights the raw whitening curve exhibited a considerable amount of noise, such that a median filter (rank 100) was applied. 150 frames (or more), before the beginning and after the end of the relevant frames showing sample compression, were included in the filtering in order to suppress artifacts in filtered curves.

2.5. Scanning electron microscopy (SEM)

For low-resolution electron microscopy the samples were rinsed briefly with water and 95% ethanol to remove residual buffer and then transferred to a custom-made aluminum vise. Subsequently they were air dried, contacted with silver paint, sputtercoated with gold, and imaged with an SEM (Model: Vega TS 5130MM, Tescan, Brno, Czech Republic). All images were recorded with an accelerating voltage of 20 keV. Higher resolution electron micrographs were obtained using a focused ion beam machine (Model: DB235 Dual-Beam Focus Ion Beam System, FEI Company, Hillsboro, OR, USA) in SEM mode with an

acceleration voltage of 10 keV. Prior to this imaging experiment, the samples were further sputtercoated with gold-palladium to reduce charging in the cracks.

3. Results

High-speed photography images of one of the trabecular bone samples during compression are presented in Fig. 2. It can be seen from these frames that the apparent strain imposed on the sample is translated into a broad range of local strains. At the failure point (at 8.4%), most of the bone structure looks more or less intact, only a few trabeculae are seen to deform and fail (cp. Figs. 2 and 3). Even at strains between 20% and 30% we find quite a few undeformed trabeculae as can be seen for example in the bottom left of the respective frames in Fig. 2. Deformed trabeculae are seen to whiten with increasing strain. This effect can be best seen in Fig. 3, which shows the magnified detail of the high-speed photography sequence marked with a black frame in the middle-left of the sample in Fig. 2. Here the whitening starts at around 4% apparent strain, very close to the yield strain of 4.8%. In Fig. 4A, corrected stress–strain data (black curve) for one of the trabecular bone sam-

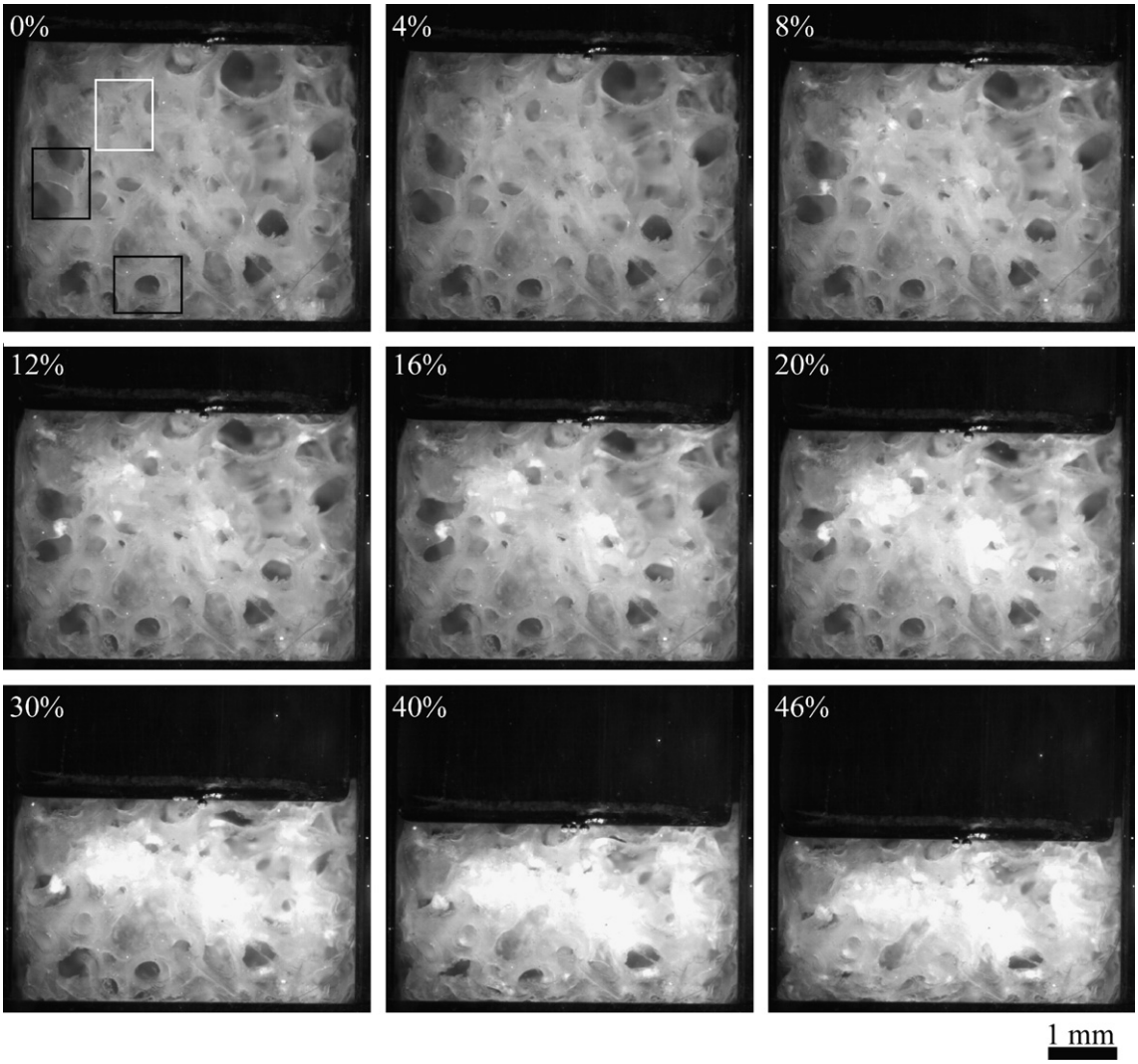

Fig. 2. High-speed photography frames of a whole trabecular bone sample under compression. Deformed trabeculae are seen to whiten. The white and black frames at 0% strain correspond to regions of interest shown in Figs. 3, 5, 7, 8 and 9.

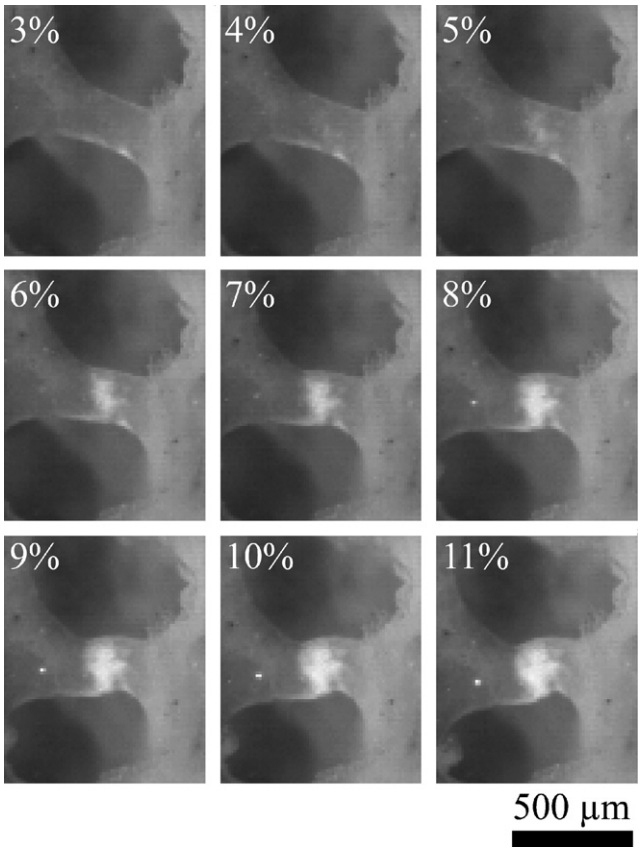

Fig. 3. Detail of the high-speed photography frames shown in Fig. 2 (black frame in the middle of the left side) at different strains showing the progression of the whitening from the plastic region to post-failure region.

ples is shown as well as the whitening progression (grey curve) with increasing strain. The stress–strain curve exhibits a non-linear toe-region and a linear elastic region, prior to yield and failure occurring at 4.8% strain and 8.4% strain, respectively, both indicated with a red line. After failure, a slight negative modulus is observed, followed by a positive slope due to compaction of the sample. In the inset in Fig. 4A both stress–strain and whitening curves are given on a different scale in order to illustrate the fact that the detected whitening steeply increases just above the yield point. The black dots on the stress–strain curve in the inset in Fig. 4A correspond to the individual images shown in Fig. 3, whereas the open circles on the stress–strain curve in Fig. 4A correspond to the high-speed photography frames of the same sample shown in Fig. 2. Comparing the high-speed photography data corresponding to the toe-region of the stress–strain curve reveals that in this region, loading results in translation and deformation of the sample. This is presumably due to the fact that the sample faces loaded in compression are not cut perfectly parallel to each other. The average stress–strain and whitening curves for all 14 samples are presented in Fig. 4B and C, respectively. Again, the whitening curve is shown on a different scale in the inset of Fig. 4C in order to illustrate the strong increase of the whitening in the plastic region, just above the yield point. Both average curves in Fig. 4B and C are very similar to the curves of the individual sample shown in Fig. 4A. Again, the stress–strain curve exhibits a non-linear toe-region and a linear elastic region, prior to yield and failure occurring at 5.6% strain and 8.9% strain, respectively, both indicated with a red line. Also, after failure, a slight negative modulus is observed, followed by a positive slope due to compaction. Similarly to the whitening of the individual sample, the average whitening exhibits a steep increase just above the yield point and finally saturates in the compaction region. After mechanical testing a few samples were secured in their recovered state and imaged with SEM. In the sample, presented in Figs. 2 and 3, we investigated several regions of interest (ROI), one of them containing the strongly deformed trabecula shown at different strains in Fig. 3, and another one containing a trabecula that

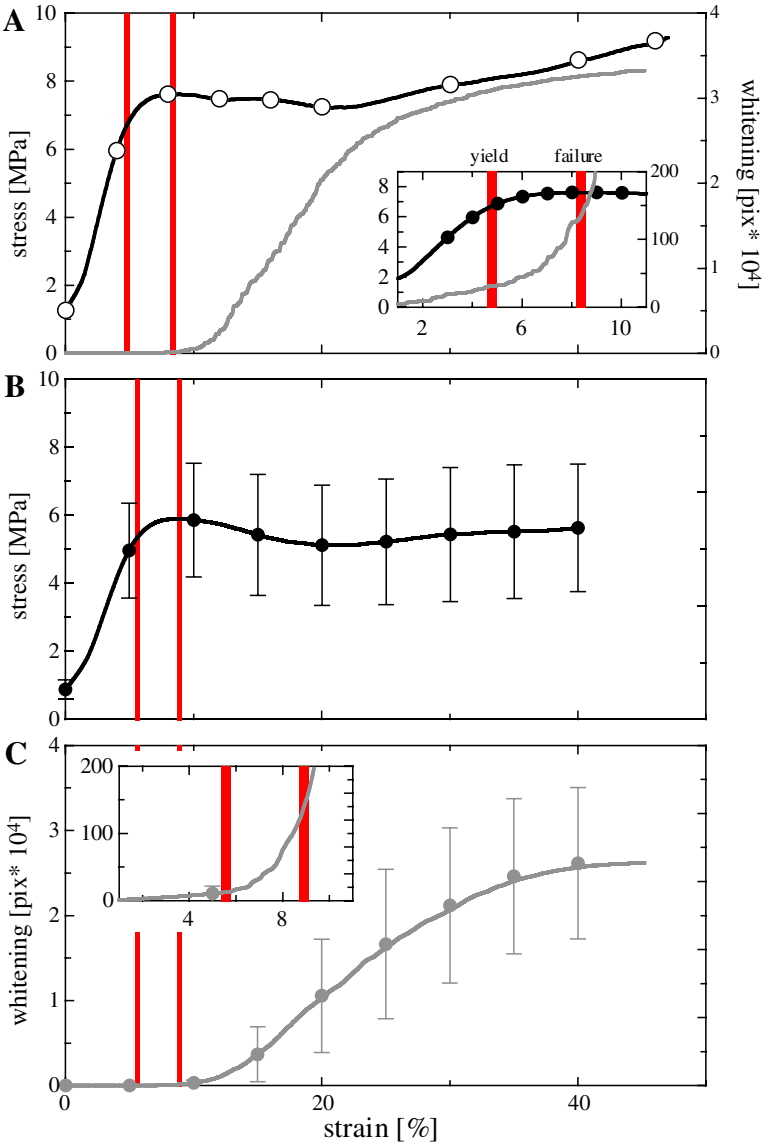

Fig. 4. Representative stress–strain and (black) whitening curves (gray) of one of the trabecular bone samples (A); the same curves are given on a different scale in the inset. Open circles on the curve and full circles in the inset correspond to the frames shown in Figs. 2 and 3, respectively. Average stress–strain (B) and whitening (C) curves for all 14 samples look similar to the curves of the individual sample. Again the whitening curve is shown on a different scale in the inset (C). The red lines (online version) indicate the yield and failure strains of the individual sample (A) and average of all samples (B, C), respectively.

did not exhibit obvious deformation even at 46% apparent strain. Both these ROIs are marked with black frames in Fig. 2. The comparison between high-speed photography and SEM of the whitened trabecula is given in Fig. 5. The corresponding morphology can be easily seen. The SE micrographs show that the whitened region is severely damaged. As can be clearly seen in Fig. 5C two microcracks are situated on the surface, both bridged by ligaments (cp. Fig. 5D). The upper crack seen in Fig. 5B and Fig. 6A was investigated in more detail with SEM at higher resolution. Relatively undamaged filaments are bridging the crack (cp. Fig. 6B), which consist of mineralized collagen fibrils, as can be seen in Fig. 6C and D. In contrast, no severe damage was seen in the region of interest (cp. Fig. 2) where no whitening is detected and no obvious deformation is seen in the high-speed photography movie. The comparison of SE micrographs with the ROI containing the trabecula with no evident deformation is presented in Fig. 7. In this ROI, no large cracks can be discerned,

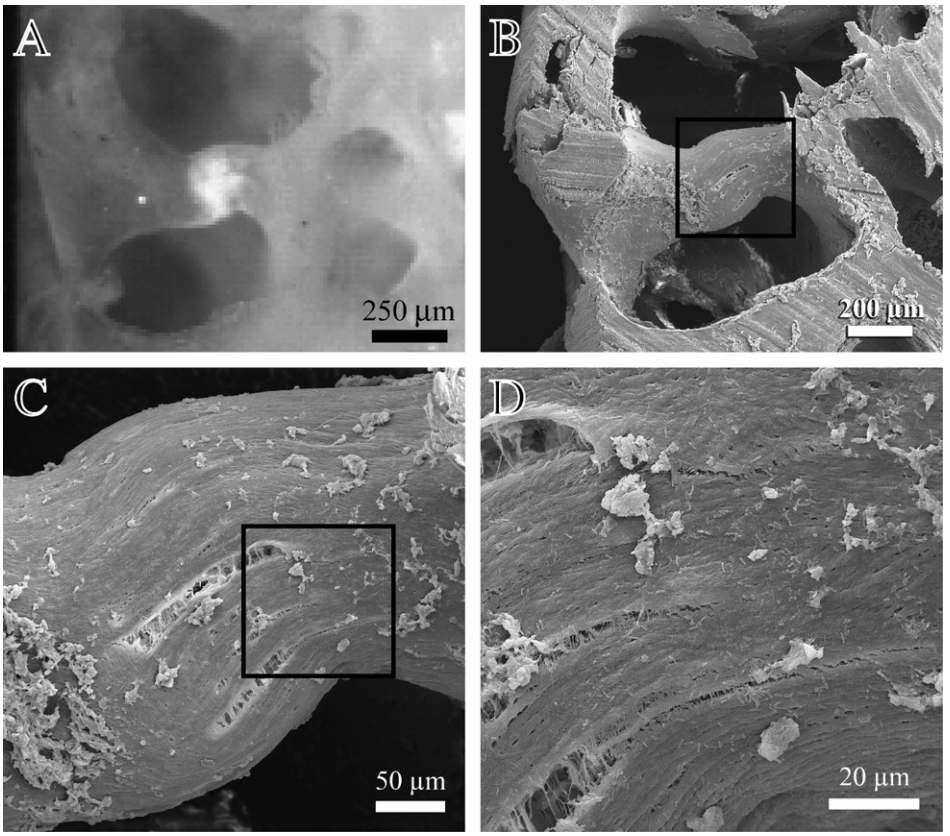

Fig. 5. Comparison between High-speed photography (A) and SEM (B–D) images of a whitened trabecula (shown in Fig. 3). Microscopic cracks with fibrilar material bridging them can be clearly seen in the SEM images, corresponding to the whitened region. The cracks are oriented parallel to the lamellar collagen structure seen on the surface off the trabecula.

however, small crack-like openings on the bone surface are observed. Interestingly we found at least one example in the high-speed photography movies of the individual sample presented in Figs. 2 and 3, where the whitening, and thus microdamage, initiates already prior to the yield point. In Fig. 8 a ROI illustrating this is presented. Upon loading the area indicated with the arrow in Fig. 8 can be seen to begin to whiten at a strain of only 2%. Upon unloading, the whitening generally decreased to some extent, which is illustrated in Fig. 9. Here the same ROI as in the SEM images in Fig. 5 is shown during compression and after recovery to 17.4% strain (cp. Fig. 9A and B). It has to be noted, however, that the shutter speed, as well as the frame rate was changed in between compression, where the sample was held for about 3 min, and recovery. In contrast, the magnified detail of another sample in Fig. 9, was recorded with exactly the same shutter and speed frame rate for compression and recovery. Here the frame rate was reduced to 60 frames/s and a recovery to 14.2% strain was recorded after compression, where the sample was held for only about 5 s. Also in this case the whitening is reduced after unloading (cp. Fig. 9C and D).

4. Discussion

Our results show that, in trabecular bone specimens, the apparent strain, imposed by a mechanical test, results in a variety of local strains. This can lead to elevated local strains, a finding reported previously also by Odgaard and co-workers, who investigated trabecular bone in compression using two video cameras [24]. Locally elevated strains have also been reported by Bay and co-workers [2], who found continuum level strains of 6% to 7% at an apparent strain of 1.8%, and by Nazarian and Müller [22]. It is interesting that Odgaard and co-workers did not report whitening of bone. It might be that the authors thought it to be an artifact rather

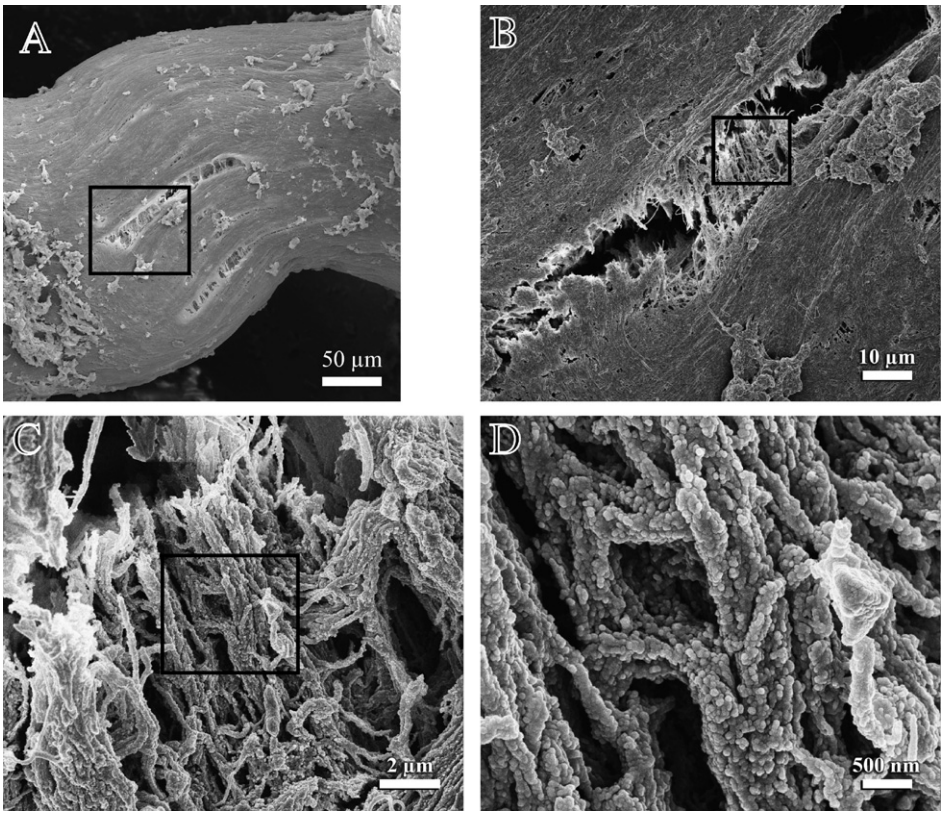

Fig. 6. Low (A) and high-resolution (SEM) images of the microscopic crack (shown in Fig. 5B–D). Fibrillar structures span the crack, coated with rounded particles, presumably hydroxyapatite crystals. Besides the protein matrix in between mineralized fibrils, it seems that mineral particles also compound different fibrils together.

than a new discovery, but it may also be that whitening is dependent on strain rate and was thus not observed. Odgaard and co-workers compressed their samples in a quasi-static mode at strain rates of 0.015%/s in contrast to our experiments where a strain rate of 50%/s was used.

The whitening images shown here are not only representative for the whole group of 14 samples but also for a total number of 30 samples of the same donor. Overall, we have so far investigated over 100 trabecular bone samples from different human donors, as well as samples retrieved from porcine and bovine bone obtained from a meat-wholesaler. Whitening was a feature we consistently observed in all of these samples. Currey [5] already hypothesized whitening to be due to microdamage but did not find conclusive evidence for this phenomenon. In our own investigation using high-speed photography and SEM, we clearly uncovered microscopic damage of whitened trabeculae, mostly in the form of delamination fractures (cp. Fig. 5), which proves this hypothesis to be correct: whitening and microscopic damage are strongly correlated. We also saw ligaments bridging the observed cracks, which consist of bundles of collagen fibrils covered with hydroxyapatite crystals (cp. Fig. 6D). These ligaments have been reported earlier for microscopic cracks in both cortical [21] and trabecular bone [7,29]. The negative control investigation of non-whitened trabeculae proved that these are neither fractured nor exhibit microscopic cracks (cp. Fig. 7). Higher resolution SEM investigation also gives some clues about the failure mechanism of healthy trabecular bone. Fig. 6D gives evidence that bone fails in the interfibrillar space, i.e. by the separation of mineralized collagen fibrils. Besides the earlier reported protein matrix holding the fibrils together in the form of a "glue" [7], it seems from these images that fibrils might also be fused by mineral crystals.

Qualitatively, we find whitened areas already in the elastic linear region of mechanical tests. This is illustrated in Fig. 8, where whitening already starts at an apparent strain of only 2%. Although we find whitening at such low apparent strains only to a limited extent, this finding has an important implication: it means that cyclic load-

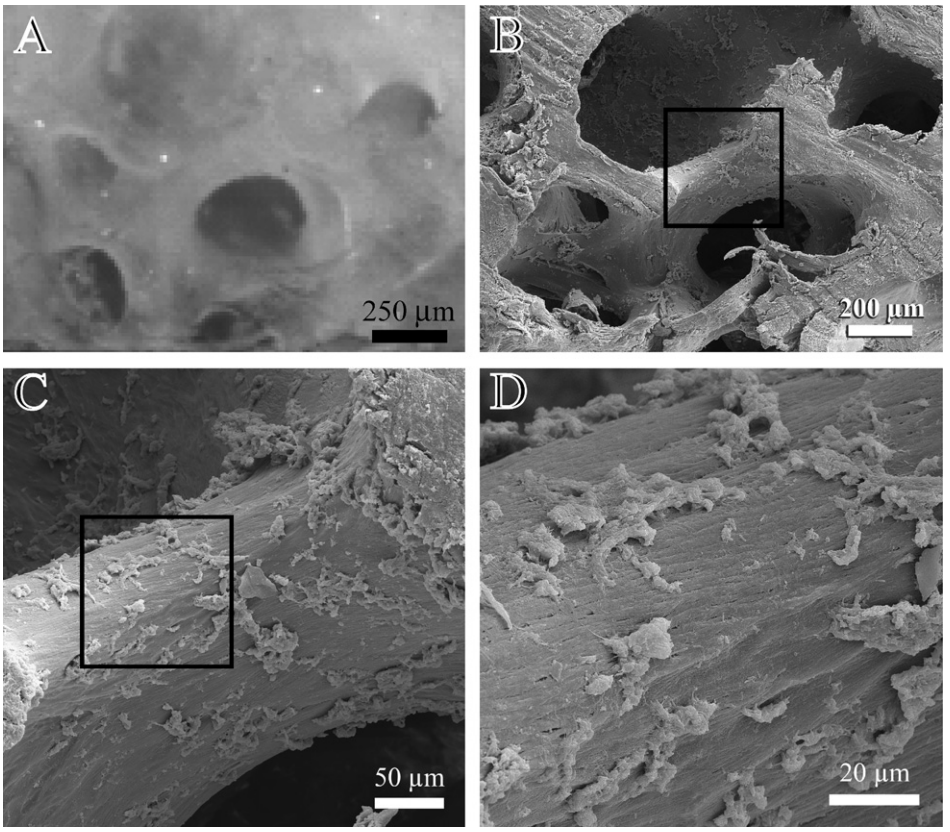

Fig. 7. Comparison between high-speed photography (A) and SEM (B–D) images of a trabecula that did not whiten (cp. Fig. 2, black frame at the bottom). The trabecula looks intact, only very small openings on the surface can be seen at a magnification of 1400× SEM (D).

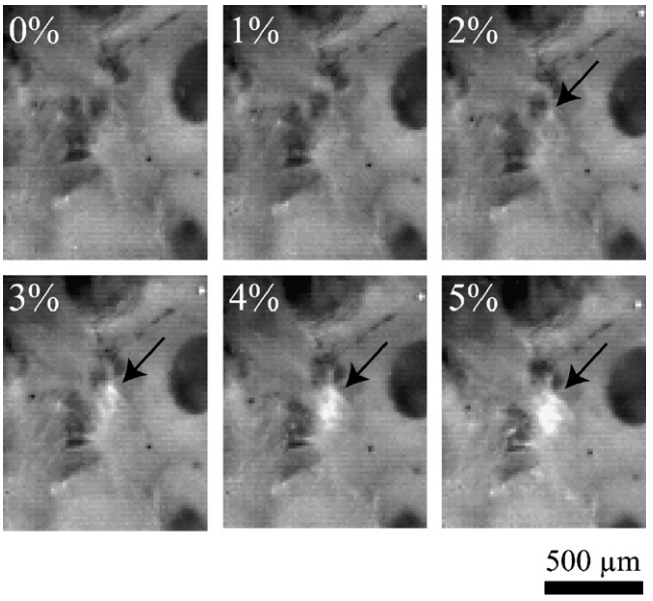

Fig. 8. Detail of the high-speed photography frames shown in Fig. 2 (white frame) at different strains showing the initiation of whitening (arrow) well below the apparent yield strain and its progression with increasing apparent strain.

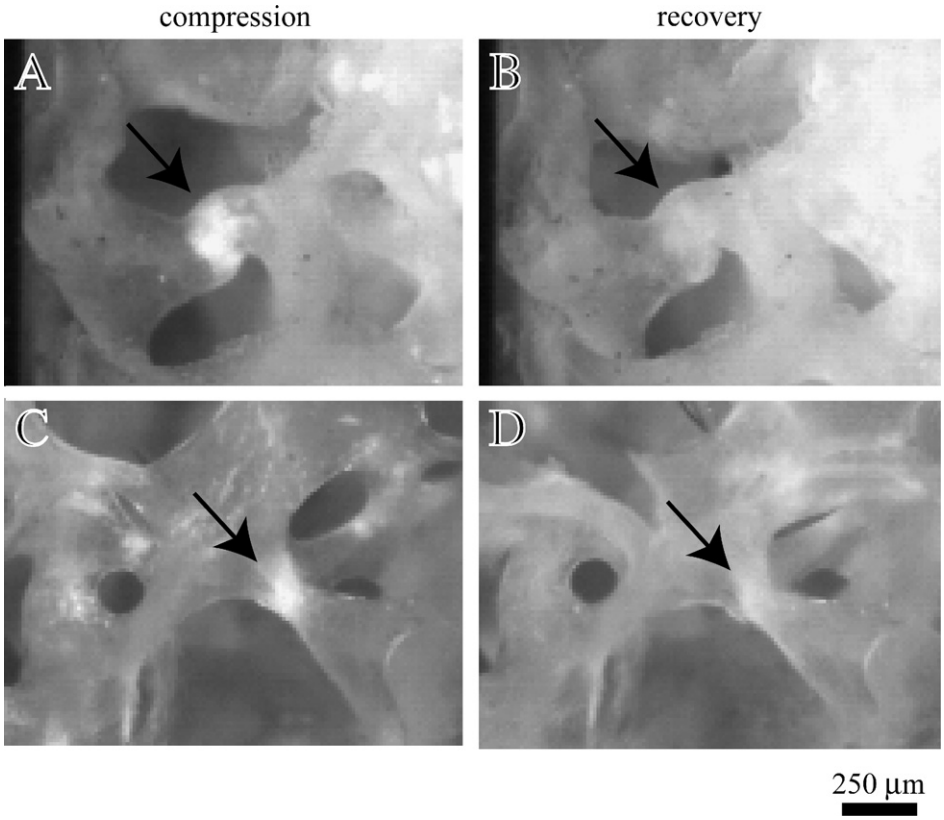

Fig. 9. Detail of two different samples during compression and recovery at 17.4% (A, B) and 14.2% (C, D) strain, respectively. In both cases the whitening (black arrows) fades after unloading.

ing of bone below the apparent yield point could already result in local overloading leading to microscopic cracks and damage. Despite the fact that this mechanism could weaken the bone, it would also provide the necessary stimulus for bone remodeling and adaptation. Generally, we found whitened regions of the bone also to be regions of high deformation, which is in agreement with the failure criterion found for cortical bone [21]: crack initiation occurs at the point of highest strain. Also Nagaraja and co-workers found that microdamage in trabecular bone is associated with high stresses and strains predicted from finite element analysis [20].

In principle, the whitening effect in bone is somewhat similar to stress-whitening due to crazing reported in polymers [28]. Crazing results in the formation of microscopic voids within a material, which scatter light in a diffuse manner. Presumably the same happens in bone where the voids are called microscopic cracks or microcracks. Similarly as in polymers, the whitening in bone fades after unloading. This effect is illustrated in Fig. 9, where two whitened regions are shown at the same strain during compression and recovery. In both cases some of the whitening is still present after unloading, but the intensity is drastically reduced. One explanation for this fading effect is that the cracks partly close after unloading.

From Fig. 4 it can be seen that the stress–strain and whitening curve of the individual sample exhibits very similar features as the average curves retrieved from all 14 samples. The whitening shows only a slight increase in the toe- and linear elastic region. It strongly increases right above the yield point and changes again to a smaller slope in the compaction region. This agrees very well with the finding that the whitening effect is due to microscopic damage; the whitening drastically increases just above the yield point in all cases, i.e. plastic deformation takes place. Although, we are not able to resolve microdamage in the great detail as in histological investigations [8,9,15,32,33], we can measure it in a quantitative manner in real-time during the compression test. It has to be noted, however, that some of the whitening detected by our algorithm may be due to general compaction of the bone samples. Since we use a global thresholding algorithm, we do not account for such effects. The contribution of compaction to the detected whitening might be reduced

by the use of algorithms that consider the local changes in brightness. The observed shape of the whitening curves presented in Fig. 4, however, cannot be explained by compaction alone, given the assumption that the whitening contribution of compaction is directly proportional to the increase in density. If assumed so, the whitening, as a function of time and at a constant strain rate, is given by the relation

$$W(t) \propto \frac{m}{V_0(1-\dot{\varepsilon}\cdot t)} \tag{1}$$

Here W denotes the whitening, t the time, m the mass of the sample, V_0 the initial volume of the sample, and $\dot{\varepsilon}$ the strain rate. If expanded into a Taylor series with $\dot{\varepsilon}\cdot t = \varepsilon$ at $\varepsilon = 0$ this transforms into

$$W(\varepsilon) \propto \frac{m}{V_0}\cdot\left[1+\varepsilon+\varepsilon^2+\varepsilon^3+\ldots\right]_{\varepsilon=0} \tag{2}$$

The nonlinear terms in Eq. (2) can be ignored in a first order approximation ($\varepsilon \ll 1$), thus the increase in whitening is almost linear.

Clearly a limitation of our approach is the fact that only a part of a bone specimen is imaged during the mechanical test, in contrast to other functional imaging approaches, where the whole 3D structure can be assessed [2,19,20,22,29,30]. However, high-speed photography is a real-time instrument, which can gather significantly more image information of a mechanical test in terms of temporal resolution compared to 3D approaches. In the 3D functional imaging experiments, usually quasi-static testing is done and only a few different stages of the sample during compression are recorded. A further limitation of the experiments presented here was the encounter of toe regions in stress–strain curves at very low strains, which we corrected for by extrapolating the linear elastic region of the stress strain curves, as also done before in other studies [29,30]. The origin of these toe regions was clearly determined to be due to slight translation and rotation of the samples, as seen in the high-speed photography movies. Apparently the sample surfaces were not cut perfectly parallel to each other. We did not precondition our samples prior to mechanical tests, which has been reported to reduce toe regions [11], as we were aiming for specimens undamaged, beyond the potentially small damage encountered during preparation. A more sophisticated sample preparation protocol should lead to better specimens and, thus, less toe regions.

In the future, we plan to include the computation of strain fields in our analysis in order to determine the true local strain needed for the formation of microscopic delamination fractures. We also consider performing a more thorough investigation of microdamage in the future using the gold standard, fluorescence labeling and sectioning for histological analysis. Overall, high-speed photography proves to be a valuable functional imaging technique that can be added with relative ease to existing mechanical testing experiments providing insight to the local failure dynamics of trabecular bone.

5. Conclusions

In this manuscript we demonstrate that combining high-speed photography and mechanical compression gives new insights into the fracture dynamics of trabecular bone. The comparison of high-speed photography data with SEM images clearly demonstrates that whitening of bone is caused by microdamage. High-speed photography is thus a tool enabling the detection of microdamage accumulation in a non-invasive and quantitative fashion during mechanical testing of trabecular bone. Qualitatively, we find elevated local strains compared to the apparent strain during compression, which is in agreement with previous studies. Elevated local strains result in whitening and thus microdamage already well below the yield point. Quantitatively, whitening and microdamage accumulation steeply increase right around the yield point and continue to increase in the plastic and post-failure region. After unloading the whitening fades, most probably due to partial crack closure. By SEM imaging we find that on the macromolecular scale bone fails through delamination and separation of mineralized collagen fibrils, which on the micro- and macroscale results in whitening.

Acknowledgements

For funding of this work we are gratefully indebted to SNF Postdoctoral fellowship PBEZ2—105116, DAAD scholarship No. D/05/42569, FWF Project No. J2395-N02, ÖAW DOC-Fellowship, NIH Grant

Number GM65354, Veeco/DI Grant Number SB030071, MRL NSF Grant Number DMR00-80034, NASA/URETI Grant Number BiMAt NCC-1-02037, USARL (ICB) Grant Number DAAD19-030D-0004, USA-RIEM (ICB) Grant Number W911QY-04-P-0516, and the NOAA National Sea Grant College Program and the US Department of Commerce (NA36RG0537, Project R/MP-92) through the California Sea Grant College System.

References

[1] Bay BK. Texture correlation: a method for the measurement of detailed strain distributions within trabecular bone. J Orthop Res 1995;13:258–67.
[2] Bay BK, Smith TS, Fyhrie DP, Saad M. Digital volume correlation: three-dimensional strain mapping using X-ray tomography. Exp Mech 1999;39:217–26.
[3] Bayraktar HH, Morgan EF, Niebur GL, Morris GE, Wong EK, Keaveny TM. Comparison of the elastic and yield properties of human femoral trabecular and cortical bone tissue. J Biomech 2004;37:27–35.
[4] Ciarelli MJ, Goldstein SA, Kuhn JL, Cody DD, Brown MB. Evaluation of orthogonal mechanical properties and density of human trabecular bone from the major metaphyseal regions with materials testing and computed tomography. J Orthop Res 1991;9:674–82.
[5] Currey JD. Bones: structure and mechanics. Princeton: Princeton University Press; 2002.
[6] Dalstra M, Huiskes R, Odgaard A, van Erning L. Mechanical and textural properties of pelvic trabecular bone. J Biomech 1993;26:523–35.
[7] Fantner GE, Hassenkam T, Kindt JH, Weaver JC, Birkedal H, Pechenik L, et al. Sacrificial bonds and hidden length dissipate energy as mineralized fibrils separate during bone fracture. Nat Mater 2005:4.
[8] Fazzalari NL, Forwood MR, Smith K, Manthey BA, Herreen P. Assessment of cancellous bone quality in severe osteoarthrosis: bone mineral density, mechanics, and microdamage. Bone 1998;22:381–8.
[9] Fyhrie DP, Schaffler MB. Failure mechanisms in human vertebral cancellous bone. Bone 1994;15:105–9.
[10] Kanis JA. Osteoporosis: a view into the next century. Neth J Med 1997;50:198–203.
[11] Keaveny TM, Guo XE, Wachtel EF, McMahon TA, Hayes WC. Trabecular bone exhibits fully linear elastic behavior and yields at low strains. J Biomech 1994;27:1127–36.
[12] Keaveny TM, Hayes WC. A 20-year perspective on the mechanical properties of trabecular bone. J Biomech Engng 1993;115:534–42.
[13] Keaveny TM, Morgan EF, Niebur GL, Yeh OC. Biomechanics of trabecular bone. Ann Rev Biomed Engng 2001;3:307–33.
[14] Keaveny TM, Wachtel EF, Kopperdahl DL. Mechanical behavior of human trabecular bone after overloading. J Orthop Res 1999;17:346–53.
[15] Lee TC, Arthur TL, Gibson LJ, Hayes WC. Sequential labelling of microdamage in bone using chelating agents. J Orthop Res 2000;18:322–5.
[16] McBroom RJ, Hayes WC, Edwards WT, Goldberg RP, White III AA. Prediction of vertebral body compressive fracture using quantitative computed tomography. J Bone Joint Surgery [Am] 1985;67:1206–14.
[17] McElhaney JH, Fogle JL, Melvin JW, Haynes RR, Roberts VL, Alem NM. Mechanical properties of cranial bone. J Biomech 1970;3:495–511.
[18] Melton III LJ, Chrischilles EA, Cooper C, Lane AW, Riggs BL. Perspective. How many women have osteoporosis? J Bone Mineral Res 1992;7:1005–10.
[19] Muller R, Gerber SC, Hayes WC. Micro-compression: a novel technique for the nondestructive assessment of local bone failure. Technol Health Care 1998;6:433–44.
[20] Nagaraja S, Couse TL, Guldberg RE. Trabecular bone microdamage and microstructural stresses under uniaxial compression. J Biomech 2005;38:707–16.
[21] Nalla RK, Kinney JH, Ritchie RO. Mechanistic fracture criteria for the failure of human cortical bone. Nat Mater 2003;2:164–8.
[22] Nazarian A, Muller R. Time-lapsed microstructural imaging of bone failure behavior. J Biomech 2004;37:55–65.
[23] Nicolella DP, Nicholls AE, Lankford J, Davy DT. Machine vision photogrammetry: a technique for measurement of microstructural strain in cortical bone. J Biomech 2001;34:135–9.
[24] Odgaard A, Hvid I, Linde F. Compressive axial strain distributions in cancellous bone specimens. J Biomech 1989;22:829–35.
[25] Ray NF, Chan JK, Thamer M, Melton III LJ. Medical expenditures for the treatment of osteoporotic fractures in the United States in 1995: report from the National Osteoporosis Foundation. J Bone Miner Res 1997;12:24–35.
[26] Rice JC, Cowin SC, Bowman JA. On the dependence of the elasticity and strength of cancellous bone on apparent density. J Biomech 1988;21:155–68.
[27] Silva MJ, Keaveny TM, Hayes WC. Load sharing between the shell and centrum in the lumbar vertebral body. Spine 1997;22:140–50.
[28] Strobl G. The physics of polymers: concepts for understanding their structures and behavior. Berlin: Springer; 1997.
[29] Thurner P, Wyss P, Voide R, Stauber M, Muller B, Stampanoni M, et al. In: Bonse U, editor. Developments in X-Ray tomography IV. SPIE Proceedings 5535. Colorado: Denver; 2004. p. 112–28.
[30] Thurner PJ, Wyss P, Voide R, Stauber M, Stampanoni M, Sennhauser U, et al. Time-lapsed investigation of three-dimensional failure and damage accumulation in trabecular bone using synchrotron light. Bone 2006;39:289–99.
[31] Ulrich D, Hildebrand T, Van Rietbergen B, Müller R, Rüegsegger P. The quality of trabecular bone evaluated with micro-computed tomography, FEA and mechanical testing. Stud Health Technol Inform 1997;40:97–112.

[32] Vashishth D, Koontz J, Qiu SJ, Lundin-Cannon D, Yeni YN, Schaffler MB, et al. In vivo diffuse damage in human vertebral trabecular bone. Bone 2000;26:147–52.
[33] Wachtel EF, Keaveny TM. Dependence of trabecular damage on mechanical strain. J Orthop Res 1997;15:781–7.
[34] WHO Assessment of osteoporotic fracture risk and its role in screening for postmenopausal osteoporosis. World Health Organization, Geneva; 1994.
[35] Williams JL, Lewis JL. Properties and an anisotropic model of cancellous bone from the proximal tibial epiphysis. J Biomech Engng 1982;104:50–6.